

## Geochemistry and Sr-Nd Isotopes of the Oligo-Miocene Bagh-e-Khoshk Granitoid in SE of the UDMA, Iran: Implications for Petrogenesis and Geodynamic Setting

S. Z. Hosseini<sup>1\*</sup>, and M. Arvin<sup>2</sup>

<sup>1</sup> Department of Geology, Payame Noor University, Tehran, Islamic Republic of Iran

<sup>2</sup> Department of Geology, Faculty of Sciences, Shahid Bahonar University of Kerman, Kerman, Islamic Republic of Iran

Received: 14 February 2020 / Revised: 4 June 2020 / Accepted: 11 July 2020

### Abstract

Oligo-Miocene Bagh-e-Khoshk granitoid stock is intruded into the Eocene volcanic rocks in the southeastern part of the Urumieh-Dukhtar Magmatic assemblage in Iran. The granitoids are mainly consisting of diorite, quartz diorite and granodioritic rock types. They are metaluminous to slightly peraluminous, medium to high K calc-alkaline, with  $\text{SiO}_2$  ranging from 50.2 to 66 wt.%. The major elements mostly define linear trends and negative slopes with increasing of  $\text{SiO}_2$ , while  $\text{K}_2\text{O}$  is positively correlated with silica. There is a higher content of Ba, Rb, Nb and Zr elements with increasing  $\text{SiO}_2$ , whereas Sr shows an opposite behavior. Primordial mantle-normalized multi-element patterns show enrichment in LILE relative to HFSE with distinctive Nb, Ta, Ti negative anomalies. These signatures are typical of subduction related magmas that formed in an active continental margin. The high Ba/La, Ba/TiO<sub>2</sub>, Ba/Nb and Th/Nb ratios emphasizes the significant involvement of fluids during subduction processes. The chondrite-normalized REE patterns of the Bagh-e-Khoshk granitoids show an enrichment in light REEs ( $(\text{La/Yb})_{\text{N}} = 3.84, 7.41$ ), very slightly HREE fractionation patterns ( $(\text{Gd/Yb})_{\text{N}} = 1.26-1.83$ ) and small positive Eu anomalies ( $(\text{Eu}_{\text{N}}/\text{Eu}_{\text{N}}^*) = 1.01, 1.44$ ) in diorites. Whole-rock Sm-Nd isotope analysis give  $\epsilon_{\text{Nd}}$  values (+2.91 to +3.29) and Sr ratios (0.7046–0.7053). The geochemical characteristics, positive  $\epsilon_{\text{Nd}}$  and low Sr ratios of the Baghe-Khoshk granitoids suggest their formation from partial melting of the mantle wedge source, at pressures below the garnet stability field, modified by fluids during subduction processes.

**Keywords:** Bagh-e-Khoshk; Granitoid; Subduction; Oligo-Miocene; Iran.

### Introduction

Urumieh-Dukhtar Magmatic assemblage (UDMA) is a part of the Zagros orogenic belt (ZOB), with a NW-SE

trend from eastern Turkey to southeast of Iran, that formed as a result of northward subduction of Neotethyan Ocean underneath the Central Iranian microcontinents (Fig. 1). UDMA has been interpreted to

\* Corresponding author: Tel: 09139943116; Fax: 03434356572; E-mail: Z\_hosseini@pnu.c.ir

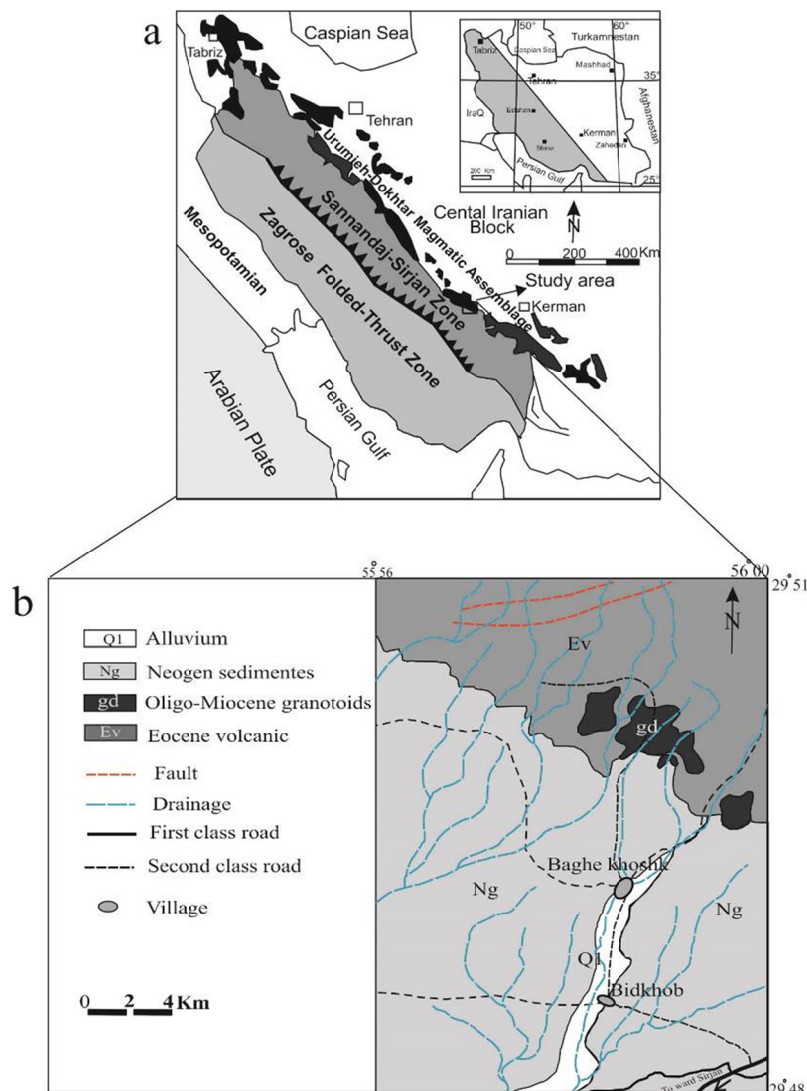


**Figure 1.** (a) Geological map of Iran illustrating major tectonic units in the Zagros orogenic belt. (b) Simplified geological map of the study area, northeast of Sirjan (modified from Geological map of Iran, 1:100000 Series, Pariz Sheet, [19]).

be an Andean-type magmatic arc that has been active from the Late Jurassic to the Miocene with peak of volcanism occurred in Middle to Upper Eocene [1, 2]. The volcanism has been followed by continental collision between the Iranian and Arabian plates, either during or before the Late Miocene time, which led to crustal shortening and thickening in the western edge of the Iranian plate and emplacement of Oligo-Miocene plutonic bodies in the UDMA [3, 4]. They are mainly consisting of granites, granodiorites, porphyritic diorites and quartz diorite that are best known for hosting world-class porphyry copper and molybdenum deposits (e.g., the Sar-Cheshmeh and Miduk mines in the Kerman region, southeast of UDMA). In this paper the focus is

on the Bagh-e-khoshk Oligo-Miocene granitoid rocks. We present field observations, petrographic studies, whole-rock geochemistry and Sr–Nd isotopes data in order to investigate its petrogenesis and tectonic significance in relationship to the regional tectonic patterns of UDMA.

#### Tectonic History

Geodynamic evolution of Iran is linked to the geologic record of initiation, spreading, and eventual destruction of the Neotethys Ocean basin that is well preserved in Iran. Sedimentary deposits record Permian-Early Triassic rifting of Gondwana along the present Zagros thrust zone which eventually led to the opening

of the Neotethys Ocean. The new ocean was expanded during Late Triassic to Early Jurassic, while pelagic marine carbonates were deposited in ZOB [5]. The ZOB consists of three parallel NW-SE trending units: Zagros folded-thrust Zone, Sanandaj-Sirjan Zone (SSZ) and Urumieh-Dukhtar Magmatic Arc (UDMA) [1, 6] (Fig. 1a). Northward subduction of the Neotethys beneath the partially accreted Sanandaj-Sirjan zone (SSZ) is recorded by voluminous Late Triassic to Cretaceous calc-alkaline I-type arc plutonic rocks. As the magmatism in the SSZ ceased in the Paleogene, arc volcanism flared up in the UDMA [7, 8]. The most likely interpretation of this northward migration of magmatism is flattening of the angle of subduction, combined with closure of the narrow back-arc basin in the Late Paleogene-Early Neogene [4, 9, 10].

Magmatism in the UDMA comprises of two distinct episodes: 1- the Paleoogene volcanics which consists of basaltic andesites, latites, analcime rich tephrites, some nepheline phonoliths and volcano-clastic rocks and 2- Oligo-Miocene plutonic rocks consisting of granodiorites, porphyritic diorites and quartz diorite. The Late Miocene-Pliocene magmatic activity comprises of some dacitic-andesitic domes and lava flows [11, 12].

The timing of final collision between the Afro-Arabian plate and Eurasia, consist of Iranian micro plates, has been the subject of considerable debate, with estimates ranging from the Paleocene [6], through the Eocene [13, 14, 15], Oligocene [16], to the Miocene [13, 17].

Seismic evidence suggests that crustal orogeny was accompanied by break off of the Neotethyan Oceanic slab under thrust the Arabian plate [18], possibly accompanied by delamination of part of the Central Iranian subcontinental lithospheric mantle [3].

## Results

### **Geological setting**

The Bagh-e-Khoshk granitoid stock, 140 km southwest of Kerman, is located in southeastern portion of the UDMA in the Dehaj-Sarduiyeh volcanic belt [19] (Fig.1). The stock is intruded into Eocene volcano-sedimentary rocks and consists mainly of diorite, quartz diorite and granodiorite. Their contacts with host rocks are commonly irregular and covered by rock debris. The host volcanic rocks experienced low-grade metamorphism and therefore mineral assemblage of calcite, epidote and chlorite appeared in them. At least three faults have been identified around the Bagh-e-Khoshk granitoid body. These lineament structures may control emplacement and exposure of granitoid and late

hypothermal alteration. Mafic microgranular enclaves (MMEs) of various types and sizes are also occasionally observed in the Bagh-e-Khoshk stock. They are angular to rounded in shape, very fine-grained compared to the host rocks and have doleritic composition. Alteration in Bagh-e-Khoshk intrusion mainly occur in central and NE parts as stock work veins.

### **Petrography**

Bagh-e-Khoshk granitoid rocks (diorite, quartz diorite and granodiorite) are generally medium to coarse grained granular to inequigranular or porphyritic textures. Mineralogically they are comprised of variable amounts of plagioclase (48-60 vol. %), quartz (<5-22 vol. %), orthoclase (3-15 vol. %), hornblende (10-26 vol. %) and biotite (3-7 vol. %). Apatite, titanite, zircon and opaque (5-7 vol. %) minerals are the main accessories. Sericite, chlorite and calcite are also locally present as secondary phases. Plagioclase, tabular in shape and 0.3 to 4 mm in size, is commonly zoned and slightly to moderately altered into sericite/clay minerals. Quartz, 0.3-1mm in size, commonly occurs as anhedral grains clustered between orthoclase and plagioclase. K-feldpars, anhedral in shape and 0.2-0.6mm in size, are slightly altered to clay minerals. Biotites, 0.2-1mm in size, are divided in to primary and secondary types. Hornblendes, 0.4- 1.2 mm in size and anhedral in shape, are moderately altered to biotite and chlorite.

### **Analytical Methods and Procedures**

A total of sixty rock samples were collected from Bagh-e-Khoshk granitoid body. After detailed petrographic studies, 31 representative samples with least alteration were selected for whole rock chemical analyses. Eighteen samples were analyzed for major elements by Wavelength-Dispersive X-ray Fluorescence Spectrometry at Sarcheshmeh mine laboratory, Iran. The rest of samples were analyzed for major and trace elements by Inductively Coupled Plasma-Atomic Emission Spectrometers (ICP-AES) and Inductively Coupled Plasma Mass Spectrometry (ICP-MS) at the Actlabs laboratory, Canada. Detection limits range within 0.01-0.1 wt% for major oxides, 0.1-10 ppm for trace elements, and 0.01-0.5 ppm for the rare earth elements. Sr and Nd isotopic analyses were carried out on selected seven samples, using geochemical criteria of whole-rock analyses, at Cape Town University in South Africa.

### **Geochemistry**

#### *Major Elements*

The Bagh-e-Khoshk intrusive rocks contain 50.20 to 66.07 wt.% SiO<sub>2</sub>, and plot in diorite, quartz diorite and

**Table 1.** Whole rock major element analyses (wt.%) of Bagh-e-Khoshk granitoid rocks. D represents diorite; Qd, quartz diorite; Gd, granodiorite and ND- not detection

Sample	DI1-6	DI-6	DI-22	DI1-22	DI1-16	DI-15	DI-20	DI1-15	DI1-20	DI1-5	DI1-14	DI1-21	DI-5	DI-8	DI1-8	DI-1
Rock type	D	D	D	D	D	D	D	D	D	Qd	Qd	Qd	Qd	Qd	Qd	Qd
<b>Major oxides (Wt%)</b>																
SiO <sub>2</sub>	50.20	50.31	50.31	51.61	52.52	52.96	53.22	53.39	53.57	54.54	54.61	54.76	54.87	55.71	55.97	56.16
Al <sub>2</sub> O <sub>3</sub>	19.62	19.06	19.54	18.77	18.61	19.66	18.46	19.71	18.46	18.08	16.77	18.41	18.02	18.35	18.26	17.81
FeO t	10.56	10.81	9.25	9.19	9.24	8.32	8.98	7.60	8.65	8.73	8.99	8.54	8.74	8.21	8.42	8.13
MgO	4.70	4.41	4.72	4.61	3.22	3.54	4.21	3.48	3.89	3.97	4.64	3.85	3.79	3.54	3.38	3.59
CaO	9.52	9.81	9.81	9.99	8.95	8.69	8.62	9.12	9.00	8.17	7.26	8.20	8.03	7.70	7.57	7.83
Na <sub>2</sub> O	2.86	3.35	3.17	2.47	3.05	3.49	3.44	2.80	2.73	2.59	1.64	2.65	3.38	3.42	2.83	3.67
K <sub>2</sub> O	0.49	0.35	0.62	0.69	0.86	0.99	1.03	1.14	1.22	1.37	2.65	1.42	1.05	1.22	1.38	1.24
TiO <sub>2</sub>	0.64	0.66	0.80	0.73	0.97	0.57	0.76	0.54	0.71	0.64	0.65	0.68	0.66	0.61	0.58	0.62
MnO	ND	0.23	0.20	ND	0.22	0.20	0.19	ND	0.23	ND	ND	ND	0.20	0.18	ND	0.16
P <sub>2</sub> O <sub>5</sub>	ND	0.27	0.31	ND	ND	0.22	0.17	ND	ND	ND	ND	ND	0.16	0.20	ND	0.18
LOI	0.99	1.47	1.69	1.34	1.57	2.05	1.33	1.72	1.17	1.29	2.13	1.12	1.79	1.52	1.24	1.31
Total	99.58	100.70	100.40	99.40	99.21	100.70	100.40	99.50	99.63	99.38	99.34	99.63	100.70	100.70	99.63	100.70
<b>Trace elements (ppm)</b>																
Sc	18.00	25.00			15.00	23.00							17.00	15.00		18.00
Be	1.00	1.00			1.00	1.00							1.00	1.00		1.00
V	244.00	255.00			170.00	211.00							189.00	168.00		167.00
Cr	40.00	< 20			< 20	60.00							< 20	< 20		60.00
Co	29.00	24.00			20.00	24.00							21.00	22.00		22.00
Ni	< 20	20.00			< 20	< 20							< 20	< 20		20.00
Cu	40.00	50.00			10.00	40.00							90.00	70.00		70.00
Zn	160.00	120.00			90.00	70.00							130.00	90.00		80.00
Ga	21.00	20.00			19.00	18.00							18.00	19.00		18.00
Ge	1.50	1.40			1.30	1.20							1.20	1.20		1.30
Rb	6.00	15.00			31.00	31.00							32.00	38.00		35.00
Sr	676.00	753.00			678.00	527.00							537.00	519.00		548.00
Y	11.10	16.90			13.70	19.90							16.40	16.00		18.10
Zr	17.00	42.00			43.00	69.00							76.00	88.00		82.00
Nb	0.50	1.70			1.70	3.10							2.90	3.00		3.40
Cs	0.50	0.70			1.10	1.40							2.40	1.20		1.50
Ba	203.00	270.00			271.00	295.00							270.00	342.00		378.00
La	9.48	17.50			11.50	12.80							14.90	11.90		19.40
(La)n	25.83	47.68			31.34	34.88							40.60	32.43		52.86
(La/Sm)n	2.51	2.78			2.65	2.22							3.13	2.41		3.09
Ce	18.40	35.00			22.80	27.50							27.70	25.50		37.90
Pr	2.33	4.33			2.87	3.56							3.17	3.21		4.49
Nd	10.20	18.30			12.20	14.90							13.00	13.20		17.70
Sm	2.37	3.95			2.72	3.61							2.98	3.10		3.94
(Sm)n	10.30	17.17			11.83	15.70							12.96	13.48		17.13
Eu	1.09	1.43			1.07	1.17							1.02	0.99		1.11
(Eu)n	14.83	19.46			14.56	15.92							13.88	13.41		15.10
Eu*	1.41	1.15			1.22	1.00							1.05	0.98		0.91

granodiorite fields on TAS diagram [20] (Fig. 1a). The TiO<sub>2</sub> contents range between 0.39 and 0.97 wt.% and are the same as values reported for subduction related rocks [21]. MgO contents vary from 1.52 to 4.64 wt.% with the highest value in diorite. The Mg# [100 MgO/(MgO + FeOt)] is between 25 to 34 for all studied rock types. Potassium contents are relatively low (< 1 wt.%) for diorites and 1% to 3 wt.% for quartz diorite and granodiorite. Na<sub>2</sub>O contents vary from 1.6% to 3.7 wt.% and K<sub>2</sub>O/Na<sub>2</sub>O ratios are < 1 except for sample number (DI-1-14), which has K<sub>2</sub>O/Na<sub>2</sub>O =1.6 high LOI>2.13.

The Bagh-e-Khoshk granitoid rocks are calc-alkaline in composition (Fig. 2b) and show metaluminous to slightly peraluminous nature on aluminum saturation index (ASI) with A/CNK values of 1-1.2 [22] (Fig. 2c). The peraluminous nature has been attributed to differentiation of olivine, pyroxene and hornblende [23] or heterogeneity of water content in the protolith [24].

Using SiO<sub>2</sub> as a fractionation index, the Bagh-e-Khoshk samples exhibit generally linear trends for most major and trace elements (Fig. 2.d-j). Al<sub>2</sub>O<sub>3</sub>, FeO<sub>t</sub>, TiO<sub>2</sub>, CaO, MgO, and P<sub>2</sub>O<sub>5</sub> show negative correlations whereas K<sub>2</sub>O increases with increasing of SiO<sub>2</sub>. CaO

**Table 1.** Ctd

Sample	DI-6	DI-6	DI-22	DI-22	DI-16	DI-15	DI-20	DI-15	DI-20	DI-5	DI-14	DI-5	DI-21	DI-5	DI-8	DI-8	DI-1
Rock type	D	D	D	D	D	D	D	D	D	Qd	Qd	Qd	Qd	Qd	Qd	Qd	Qd
<b>Trace elements (ppm)</b>																	
Eu*		1.41	1.15			1.22	1.00							1.05	0.98	0.91	
Gd		2.35	3.68			2.65	3.53							2.95	3.08	3.54	
(Gd)n		7.68	12.03			8.66	11.54							9.64	10.07	11.57	
(Gd/Yb)n		1.81	1.83			1.56	1.51							1.44	1.53	1.62	
Tb		0.35	0.55			0.43	0.57							0.47	0.47	0.53	
Dy		2.05	3.12			2.50	3.39							2.82	2.70	3.20	
Ho		0.38	0.61			0.47	0.68							0.57	0.56	0.63	
Er		1.06	1.77			1.37	2.01							1.61	1.61	1.85	
Tm		0.16	0.26			0.20	0.30							0.24	0.24	0.27	
(Yb)n		4.23	6.57			5.56	7.66							6.69	6.57	7.14	
Yb		1.05	1.63			1.38	1.90							1.66	1.63	1.77	
Lu		0.17	0.24			0.22	0.29							0.27	0.26	0.28	
Hf		0.50	1.00			1.40	2.00							2.10	2.30	2.30	
Ta		0.04	0.12			0.13	0.22							0.20	0.21	0.26	
Pb		17.00	9.00			12.00	8.00							28.00	15.00	16.00	
Th		0.46	1.69			2.39	2.78							2.53	3.91	5.35	
U		0.14	0.55			0.79	0.74							0.74	1.10	1.52	

**Table 1.** Ctd

Sample	DI-12	DI-12	DI-17	DI-2	DI-1-9	DI-3	DI-25	DI-4	DI-1	DI-25	DI-3	DI-4	DI-10	DI-10	DI-11	DI-13	DI-13
Rock type	Qd	Qd	Qd	Qd	Qd	Qd	Qd	Qd	Qd	Qd	Gd	Gd	Gd	Gd	Gd	Gd	Gd
<b>Major oxides (Wt%)</b>																	
SiO <sub>2</sub>	56.77	56.26	56.68	57.07	57.18	57.21	57.73	57.92	57.96	57.96	59.08	60.04	61.40	61.55	62.50	65.12	66.07
Al <sub>2</sub> O <sub>3</sub>	18.05	18.25	17.70	17.47	18.22	17.89	17.84	17.41	19.07	17.61	17.28	17.22	16.29	16.97	16.49	15.53	15.25
FeO t	7.16	7.01	9.55	7.21	7.55	7.76	7.19	7.28	7.37	6.86	7.34	6.97	6.01	5.88	6.28	4.31	4.53
MgO	3.16	3.36	3.63	3.24	3.22	3.15	3.02	2.82	2.04	2.78	2.89	2.42	2.44	2.49	2.31	1.68	1.65
CaO	7.14	7.16	6.55	7.35	7.71	7.01	6.72	6.49	7.36	6.54	6.68	6.49	5.75	5.36	4.77	3.91	3.71
Na <sub>2</sub> O	3.70	3.05	2.25	2.62	2.09	3.32	3.35	3.46	2.87	2.94	2.90	2.90	3.46	2.83	2.44	3.03	3.56
K <sub>2</sub> O	1.57	1.74	0.58	1.78	1.66	1.15	1.89	1.67	1.62	2.05	1.25	1.74	2.36	2.73	2.46	3.01	2.86
TiO <sub>2</sub>	0.57	0.57	0.80	0.59	0.64	0.60	0.59	0.59	0.59	0.50	0.53	0.50	0.45	0.45	0.47	0.35	0.39
MnO	0.16	ND	0.22	0.19	0.17	0.13	0.15	0.11	0.17	0.19	ND	ND	0.14	0.17	ND	ND	0.09
P <sub>2</sub> O <sub>5</sub>	0.18	ND	ND	ND	ND	0.19	0.17	0.17	ND	ND	ND	ND	0.14	ND	ND	ND	0.10
LOI	2.12	1.89	1.88	1.08	0.94	2.25	2.05	1.94	0.34	1.85	1.48	1.37	1.65	1.28	1.79	1.49	1.75
Total	100.60	99.29	99.84	98.60	99.38	100.70	100.70	99.85	99.39	99.28	99.43	99.65	100.10	99.71	99.51	98.43	99.97
<b>Trace elements (ppm)</b>																	
Sc	14.00					15.00	17.00	14.00					12.00				8.00
Be	1.00					1.00	1.00	1.00					1.00				2.00
V	145.00					143.00	158.00	134.00					110.00				74.00
Cr	< 20					< 20	70.00	80.00					100.00				110.00
Co	17.00					19.00	17.00	16.00					10.00				10.00
Ni	< 20					< 20	< 20	< 20					< 20				< 20
Cu	10.00					140.00	70.00	120.00					50.00				60.00
Zn	80.00					170.00	80.00	60.00					180.00				90.00
Ga	17.00					18.00	18.00	17.00					17.00				15.00
Ge	1.20					1.60	1.20	1.60					1.30				1.20
Rb	40.00					32.00	58.00	59.00					74.00				81.00
Sr	589.00					509.00	504.00	448.00					435.00				355.00
Y	15.40					17.60	17.10	17.80					16.00				17.20

and Al<sub>2</sub>O<sub>3</sub> trends indicate fractionation of An riched plagioclase while decreasing of FeO<sub>t</sub> and TiO<sub>2</sub> show Ti bearing magnetite fractionation. The MgO trend with low Mg# reveals differentiation of Fo rich olivin before

rising and emplacement of magma in crust [25]. These chemical variations indicate the importance role of fractional crystallization in the Bagh-e-Khoshk magmatic evolution.

**Table 1.** Ctd

Sample	DI-12	DI1-12	DI1-17	DI1-2	DI1-9	DI-3	DI-25	DI-4	DI1-1	DI1-25	DI1-3	DI1-4	DI1-10	DI1-10	DI1-11	DI1-13	DI1-13
Rock type	Qd	Qd	Qd	Qd	Qd	Qd	Qd	Qd	Qd	Qd	Gd	Gd	Gd	Gd	Gd	Gd	Gd
<b>Trace elements (ppm)</b>																	
Zr	63.00					101.00	95.00	113.00					118.00				136.00
Nb	3.30					3.60	3.50	3.60					3.90				4.50
Cs	1.10					1.20	1.20	2.90					2.60				1.10
Ba	462.00					539.00	436.00	451.00					540.00				717.00
La	12.90					19.10	14.50	17.00					13.80				10.40
(La)n	35.15					52.04	39.51	46.32					37.60				28.34
(La/Sm)n	2.37					3.41	2.80	3.10					2.88				2.14
Ce	30.10					37.10	29.60	34.60					28.00				24.30
Pr	3.85					4.31	3.61	4.16					3.40				3.21
Nd	16.30					17.10	14.80	16.10					13.70				13.40
Sm	3.41					3.51	3.25	3.44					3.00				3.04
(Sm)n	14.83					15.26	14.13	14.96					13.04				13.22
Eu	1.07					1.06	0.98	1.07					0.88				0.86
(Eu)n	14.56					14.42	13.28	14.56					11.95				11.69
Eu*	1.04					0.96	0.92	0.95					0.91				0.89
Gd	2.92					3.23	3.24	3.45					2.88				2.85
(Gd)n	9.54					10.56	10.59	11.27					9.41				9.31
(Gd/Yb)n	1.49					1.34	1.40	1.37					1.46				1.26
Tb	0.45					0.52	0.50	0.53					0.45				0.46
Dy	2.62					3.08	2.93	3.12					2.67				2.77
Ho	0.53					0.63	0.58	0.64					0.53				0.56
Er	1.55					1.86	1.76	1.92					1.55				1.68
Tm	0.23					0.29	0.27	0.30					0.23				0.27
(Yb)n	6.41					7.86	7.58	8.23					6.45				7.38
Yb	1.59					1.95	1.88	2.04					1.60				1.83
Lu	0.26					0.31	0.29	0.33					0.26				0.29
Hf	1.80					2.30	2.60	2.70					3.10				3.80
Ta	0.22					0.29	0.29	0.27					0.30				0.46
Pb	12.00					15.00	10.00	6.00					14.00				22.00
Th	3.63					4.81	4.84	4.42					5.49				9.84
U	1.34					1.27	1.34	1.22					1.25				2.93

*Trace element*

Trace element composition of thirteen samples of Bagh-e-Khoshk granitoid rocks are listed in Table 2. Rb (5 to 81 ppm) and Ba (200 to 700 ppm) contents show positive correlation with increasing of SiO<sub>2</sub>. Sr concentration changes from 765 ppm in diorite to 435 ppm in granodiorite and show negative correlation with increasing of silica content. Rb, Sr and Ba are the most useful trace elements for evaluation of fractional crystallization in granitoids [26]. Sr is incompatible for most common minerals except plagioclase, similarly Ba and Rb are partitioned in K-feldspar [27]. Consequently, Ba/Sr and Rb/Sr ratios increase and decrease with crystallization of plagioclase and K-feldspar respectively. So, the increase of ratios from diorite to granodiorite in the Bagh-e-Khoshk granitoids is an indication of plagioclase fractionation. Co and V show a negative correlation with increasing silica content and

behave as compatible elements. The decrease in Co, V and TiO<sub>2</sub> together with increasing SiO<sub>2</sub> provides evidence for the fractionation of Fe-Ti oxides.

In the primordial mantle-normalized trace element diagrams, the Bagh-e-Khoshk granitoid rocks generally show an enrichment in large ionic lithophile elements (LILEs, e.g. Rb, Ba, and K); but they are depleted (except in some quartz diorites and granodiorites) in high field strength elements (HFSEs, e.g. Nb, Ta, Ti, Zr, and Hf) (Fig 3.b,d). The non-existence negative Zr and Hf anomalies may be related to the aggregation of Zr-bearing minerals such as zircon.

Chondrite-normalized rare earth element (REE) patterns for the Bagh-e-Khoshk granitoid rocks are shown in figures 3a and c. The light rare earth elements (LREE) show 40-80 times the chondrite values and the patterns exhibit fractionation between LREE and HREE ([La/Yb]n = 3.84-7.41) and very slightly HREE

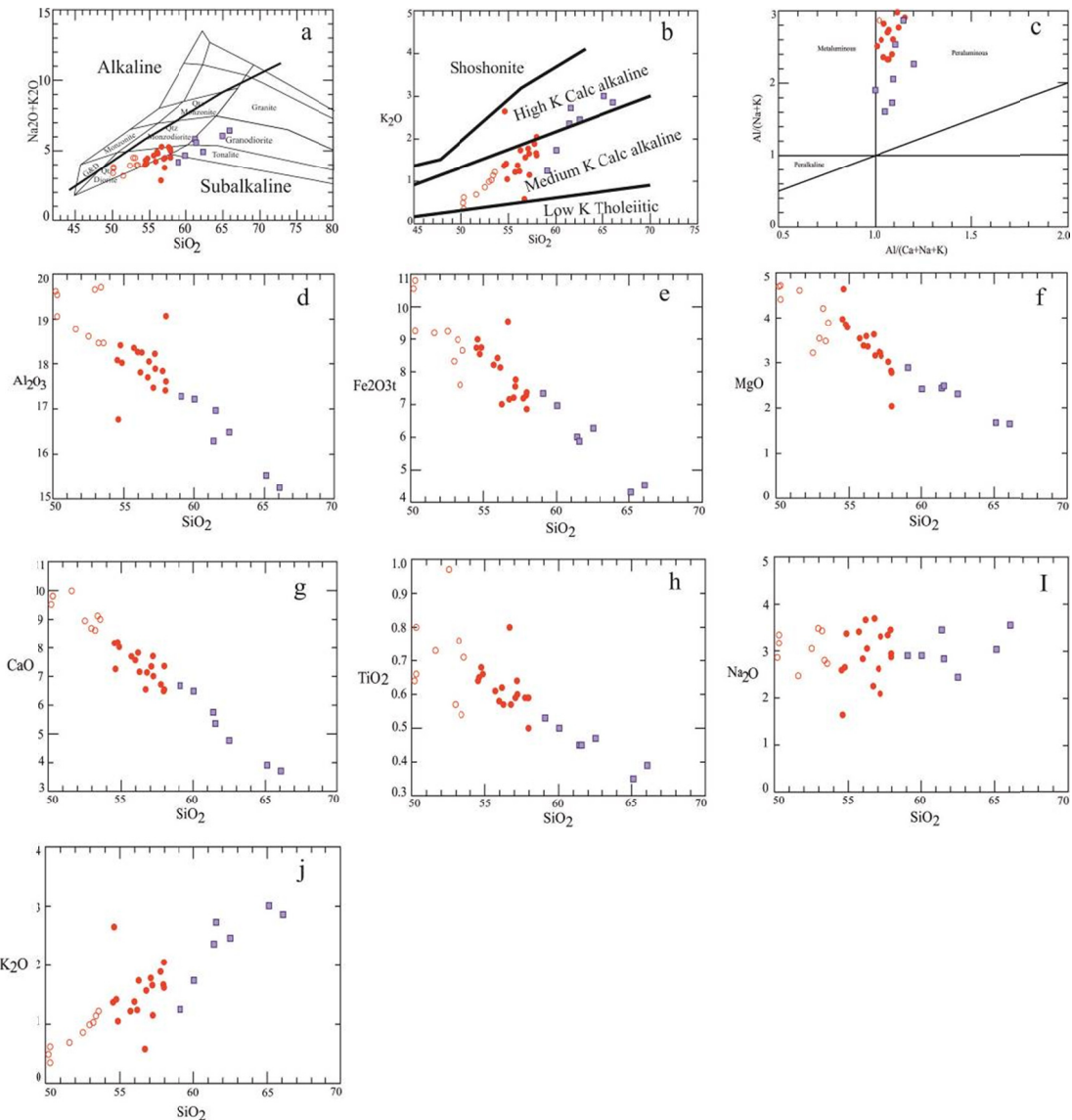


**Figure 2.** Petrochemical classification and geochemical characteristics of Bagh-e-Khoshk granitoid rocks. (a) Total alkalis versus silica diagram (TAS, after [20]); (b)  $K_2O$  versus  $SiO_2$  classification diagram [26]; (c)  $A/NK$  versus  $A/CNK$  [22] and (d–j) Covariation diagrams of  $SiO_2$  versus selected whole-rock major oxides. Symbols: open circles- diorite, solid circles- quartz diorite and open square- granodiorite.

fractionation patterns ( $[Gd/Yb]_n=1.26\text{--}1.83$ ). This ratios and the HREE patterns are indicative of melting at pressures below the garnet stability field [27]. Moreover, diorites show positive Eu anomalies with  $(Eu/Eu^*)_n$  values between 1.01 and 1.44 but quartz diorite and granodiorite have  $(Eu/Eu^*)_n$  values less than 1 with slightly negative Eu anomalies; indicating the role of plagioclase during fractional crystallization processes [29,14]. Also, the concave-upwards REE patterns between the middle and HREE (Fig. 3 a,c) and decreasing Dy/Yb ratios with increasing  $SiO_2$  indicate fractional crystallization of plagioclase under low

pressure [30].

#### Whole -rock Sr-Nd Isotopes

Representative Sr-Nd isotope data of seven selected Bagh-e-Khoshk granitoid samples are listed in Table 2. They have relatively homogeneous Nd isotopic compositions with  $\epsilon_{Nd}$  from +2.91 to +3.29 and  $^{87}Sr/^{86}Sr$  ratios of 0.7046–0.7053. The data are plotted in figure 4 and compared with existing Sr–Nd isotopic data [33] for Eocene basaltic rocks of UDMA. The resemblance of  $^{87}Sr/^{86}Sr$  ratios in the Eocene volcanic rocks with Bagh-e-Khoshk granitoid rocks reflects

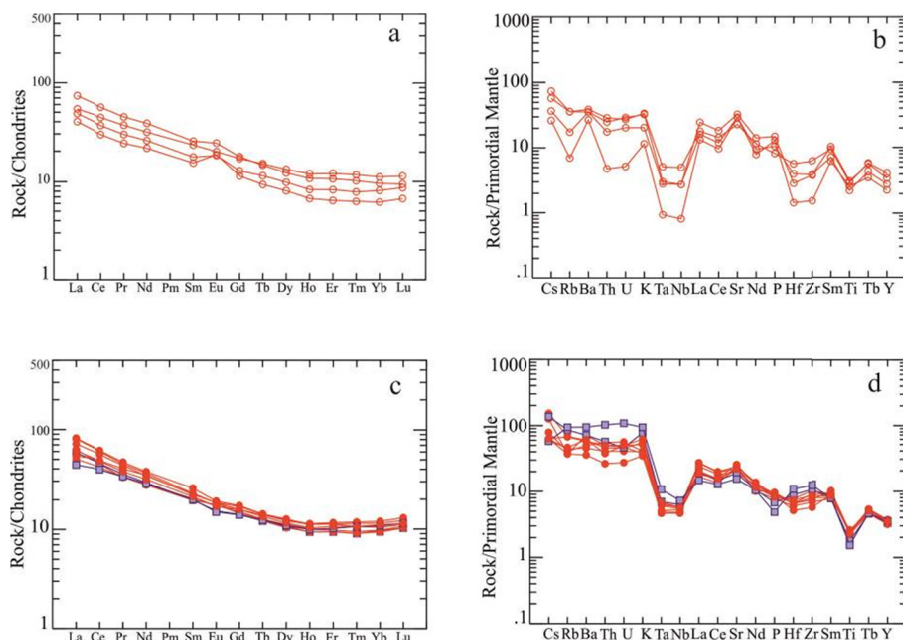


**Figure 3.** Chondrite-normalized REE patterns and primordial mantle-normalized spider diagrams for Bagh-e-Khoshk granitoid rocks. Chondrite and primordial mantle values are [31,32] respectively. Symbols as in figure 2.

**Table 2.** Rb–Sr and Sm–Nd isotopic data of seven selected Bagh-e-Koshk granitoid samples.

Sample	Rb	Sr	87Rb/Sr <sub>86</sub>	87Sr/86Sr	(87Sr/86Sr)I	Nd	Sm	147Sm/144Nd	143Nd/144	(143Nd/144Nd)I	εNd Nd
DI-1	35	548	0.185	0.704710	0.70426	17.7	3.94	0.13454	0.512731	0.51258	3.17
DI-4	59	448	0.381	0.704653	0.70373	16.1	3.44	0.12914	0.512731	0.51259	3.29
DI-8	38	519	0.212	0.704833	0.70432	13.2	3.1	0.14194	0.512731	0.51257	3.01
DI-10	74	435	0.492	0.705150	0.70395	13.7	3	0.13235	0.512731	0.51258	3.22
DI-13	81	355	0.660	0.705320	0.70372	13.4	3.04	0.13712	0.512731	0.51258	3.12
DI-20	31	527	0.170	0.704936	0.70452	14.9	3.61	0.14643	0.512731	0.51257	2.91
DI-25	58	504	0.333	0.705094	0.70429	14.8	3.25	0.13272	0.512731	0.51258	3.21

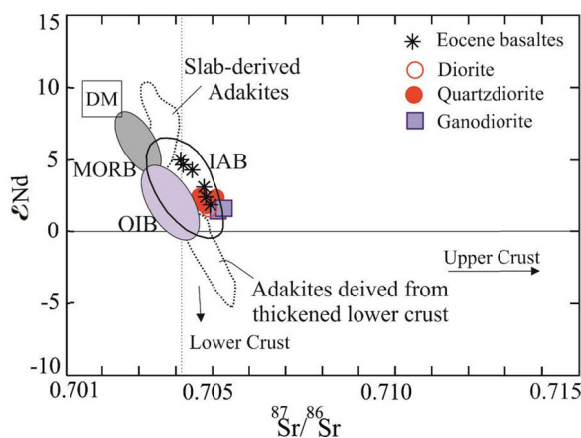


**Figure 4.** εNd–( $^{87}\text{Sr}/^{86}\text{Sr}$ ) diagram of seven selected Bagh-e-Khoshk granitoid samples

similarity in their magma source regions.

The very similar initial Sr and Nd isotopic compositions in the Bagh-e-Khoshk samples suggest they are co-genetic, deriving from the same parental

magmas. Positive εNd values indicate a source region with high Sm/Nd ratio and suggest that the Bagh-e-Khoshk granitoid rocks source was either the mantle and/or juvenile crustal material derived from the mantle.

[34] argued that lower Sr ratios of productive igneous rocks generally reflect mantle source affinities or a deep crustal mafic source with amphibole and/or garnet as source minerals. The low  $^{87}\text{Sr}/^{86}\text{Sr}$  ratios of Bagh-e-Khoshk granitoid rocks indicate that they have not been affected by shallow crustal assimilation [35].

## Discussion

### Magma genesis

Bagh-e-Khoshk granitoid rocks are enriched in LILE whereas depleted in Nb, Ta and Ti. These are typical signature of subduction related magmas [21]. Metasomatized lithospheric mantle xenoliths also tend to have negative Ta and Ti anomalies [36]. In Table 3, High Ba/La (15-20), Th/La (.5-1), La/Nb (2-10), Ba/Ta (1200-2000) and Ba/Nb (90-170) ratios of Bagh-e-Khoshk granitoid rocks are significantly same as orogenic magma. According to [37], Ba/Ta ratio greater than 450 is the single most diagnostic geochemical

characteristic of the orogenic magmas. The geochemical characteristics of Bagh-e-Khoshk granitoid rocks such as SiO<sub>2</sub>, Yb (an average of 1.8 ppm) and Y (an average of 17 ppm) contents, REE patterns (La/Yb=3.8-7.3) indicate their calc-alkaline nature rather than adakitic one. Also, in Sr/Y versus Y and La<sub>n</sub>/Yb<sub>n</sub> versus Yb<sub>n</sub> discrimination diagrams (Fig. 5), they plot in classical arc volcanic rocks field. Calc-alkaline mafic-intermediate orogenic magmas can be derived from the magma that formed by partial melting of metasomatized mantle source [38].

The chemical composition of Bagh-e-Khoshk granitoid rocks: SiO<sub>2</sub> (50 to 55 wt%), negative anomalies of Nb-Ta and Ti, enrichment in incompatible elements (e.g. Th, U, K, Rb and LREE), REE fractionation, Rb (<15), high Sr>520 and Ba>200, Rb/Sr ratio < 0.1, isotopic signatures of  $\epsilon\text{Nd} = +1.78$  and low  $^{87}\text{Sr}/^{86}\text{Sr}$  ratios (<0.7049); all emphasize their possible derivation from metasomatized mantle source [40]. As it has been shown in figure 4, the Bagh-e-

**Table 3.** Comparison of the incompatible trace element ratios of Bagh-e-Khoshk granitoid with those of orogenic andesite, oceanic rocks, lower, upper and bulk continental crust compositions.

	Orogenic Andesite <sup>a</sup>	Baghe- khoshk granitoid <sup>b</sup>	Average E MORB <sup>a</sup>	Average N MORB <sup>a</sup>	Lower CC <sup>a</sup>	Upper CC <sup>a</sup>	Bulk CC <sup>a</sup>
<b>La/Nb</b>	>2	2-10	0.8	1.2	4.4	2.6	2.5
<b>Ba/Nb</b>	>30	90-170	7.3	4	151	52.3	57
<b>Ba/Ta</b>	>450	1200-2000	129.6	59	ND	697.8	651.4
<b>Ba/La</b>	>15	15-40	9.5	3.3	>15	20.3	22.8
<b>Th/La</b>	>0.14	0.5-1	0.11	0.05	>0.14	0.34	0.28

ND: no Ta data present

CC: Continental Crust.

<sup>a</sup> [39].

<sup>b</sup>This study

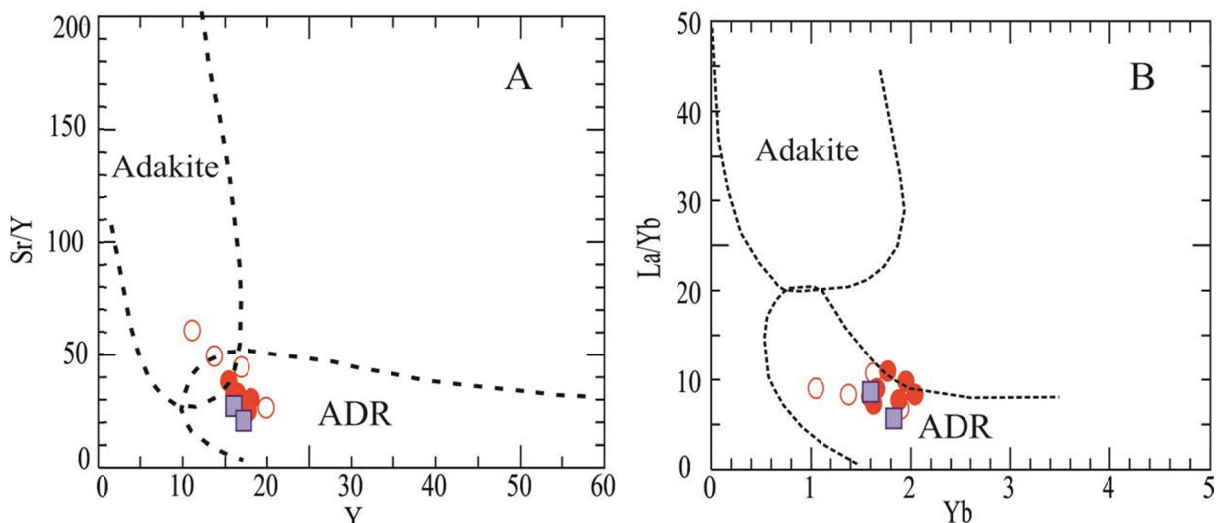


**Figure 5.** Plots of (A) Sr/Y versus Y and (B) La/Yb versus. Yb (modified after [41]) to distinguish adakite from normal arc andesite, dacite and rhyolite (ADR) lavas

Khoshk samples have Sr and Nd isotopic compositions very similar to those of normal island arc basalts and Eocene basalt in the Sarcheshmeh area (unpublished data) which is pointing to melting of a mantle wedge; followed by magmatic differentiation. Also, Sr and Nd isotopic ratios of Bagh-e-Khoshk granitoid rocks (Table 2) suggest all the rock types were genetically derived from the same source materials and that the crustal contamination/or mixing with crustal-derived magma have no roles in their formation. Constant values of  $\epsilon_{\text{Nd}}$  and Sr ratios with variation of SiO<sub>2</sub> also indicate a slight or no of crustal contamination during fractional crystallization.

The contribution of subduction components in the genesis of the Bagh-e-Khoshk granitoid rocks has been shown in a Th/Yb versus. Ta/Yb diagram [42] (Fig. 6), where the rocks show high Th/Yb contents. This is

predominantly related to the addition of a subduction-derived component to the arc wedge mantle [43]. Also, Th/Zr (0.03–0.07), Rb/Y (0.5–5), Ba/Nb (90–160) and Ba/Th (70–160) ratios in the Bagh-e-Khoshk granitoid rocks, infer the participation of both fluids and melts in the mantle metasomatism [44]. Moreover, high Ba/La ratios (Fig. 7), as well as high Ba/TiO<sub>2</sub>, Ba/Nb and Th/Nb ratios suggest significant fluid involvement during magma generation. There is a general consensus that the described REE and multi elements pattern is mainly controlled by fluid and element partitioning from the slab to the mantle wedge [45].

#### Geodynamic implications

As it was stated above the geochemical features of Bagh-e-Khoshk granitoid rocks show a strong affinity with calc-alkaline arc magmas. It is generally accepted

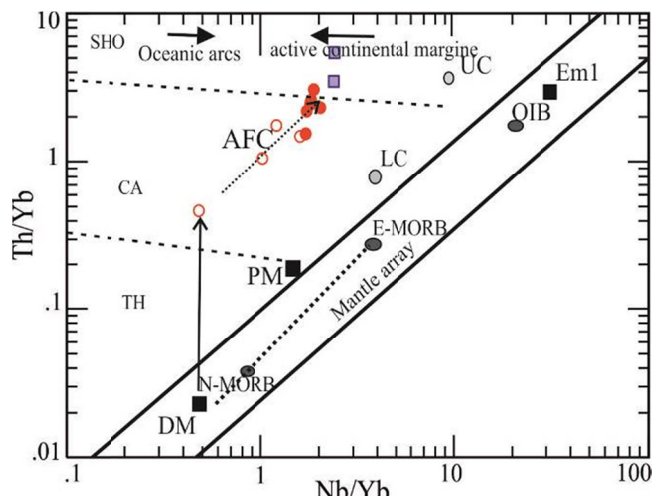


**Figure 6.** Th/Yb versus. Ta/Yb diagram [46]. N-MORB, E-MORB, OIB, Em1 and primordial mantle (PM) are from [31]; average lower crust (LC) and upper crust (UC) are from [47]

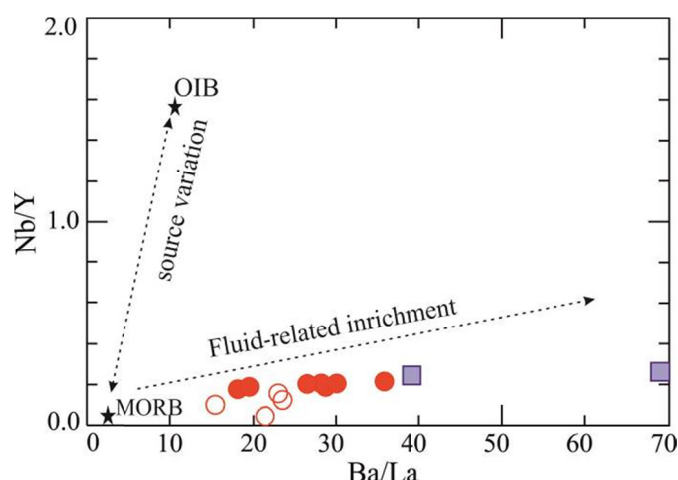


**Figure 7.** Nb/Y versus. Ba/La diagram for Bagh-e-Khoshk granitoid rocks [48]. OIB and MORB datas from [31]

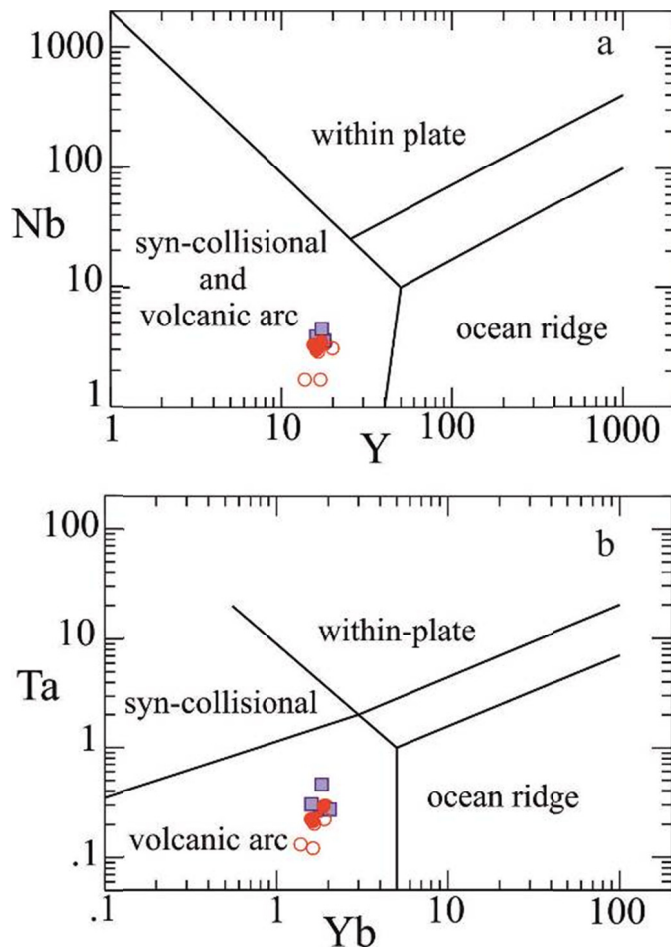


**Figure 8.** Tectonic discrimination diagrams for the Bagh-e-Khoshk granitoids [50]

that UDMA was an active Andean-like margin during Eocene to Miocene time and characterized by calc alkaline magmatism [6,10]. It represents a magmatic arc overlying the slab of Neo-Tethyan oceanic lithosphere which was subducted northwards beneath the Central Iranian microcontinent until the Miocene [10, 49]. The Bagh-e-Khoshk granitoids has geochemical characteristics of normal island arc basalts. In  $\epsilon_{\text{Nd}}$  versus ( $^{87}\text{Sr}/^{86}\text{Sr}$ ) diagram (Fig. 4) the granitoid rocks have Sr and Nd isotopic composition very similar to those of normal island arc basalts. In the Nb versus Y and Ta versus Yb granitoid tectonic discrimination diagrams, the Bagh-e-Khoshk granitic rocks display a continental arc setting (Fig. 8). The Miocene magmatism of Bagh-e-Khoshk was formed by subduction processes in mantle wedge and emphasizes collision between the Arabian and Central Iranian plates along the Zagros suture zone happened during or after Miocene as it was explained by [1, 10, 49].

### Conclusion

The Bagh-e-Khoshk I-type granitoid body is comprises of diorite, quartz diorite and granodioritic rocks. They are metaluminous to weakly peraluminous and calc-alkaline in composition. The granitoids display trace element features, such as LILE enrichment and marked Nb, Ta and Ti negative anomalies, typical of the magmatism related to a subduction zone. Tectonic discrimination diagrams reveal that the Bagh-e-Khoshk granitoid formed in a continental arc regime during subduction of the Neo-Tethys oceanic lithosphere underneath the Central Iranian microcontinent.

The geochemical and isotopic data ( $\epsilon_{\text{Nd}} = +2.91$  to  $+3.29$ , and  $^{87}\text{Sr}/^{86}\text{Sr}$  ratios (0.7046 to 0.7053) of Bagh-e-Khoshk granitoids shows their derivation from an arc basalt that was resulted of partial melting of a mantle source which was modified by slab-derived components from an earlier subduction event. Melting probably occurred outside of the garnet stability field. Formation

of Bagh-e-Khoshk granitoids in Miocene emphasizes collision between the Arabian and Central Iranian plates along the Zagros suture zone happened during or after Miocene.

## References

- Berberian M. and King G.C.P. Towards a palaeogeography and tectonic evolution of Iran. *Can. J. Earth Sci.* **18**: 210–265 (1981).
- Arvin M., Pan Y., Dargahi S., Malekizadeh A. and Babaei A. Petrochemistry of the Siah-Kuh granitoid stock southwest of Kerman, Iran: Implications for initiation of Neotethys subduction. *J. Asian Earth Sci.* **30**: 474–489 (2007).
- Shomali Z.H., Keshvari F., Hassanzadeh J. and Mirzaei N. Lithospheric structure beneath the Zagros collision zone resolved by non-linear teleseismic tomography. *Geophys. J. Int.* **187**: 394–406 (2011).
- Richards, J.P. Tectonic, magmatic, and metallogenic evolution of the Tethyan orogen: From subduction to collision. *Ore. Geol. Rev.* **70**: 323–345 (2015).
- Wilmsen M., Fürsich F.T., Seyed-Emami K., Majidifard M.R. and Taheri J. The Cimmerian orogeny foreland perspective: *Geophys. Res. Ab.* **9**: 02690 (2007).
- Alavi M. Regional stratigraphy of the Zagros folded-thrust belt of Iran and its proforeland evolution. *Am. J. Sci.* **304**: 1–20 (2004).
- Castro A., Aghazadeh M., Badrzadeh Z. and Chichorro M. Late Eocene-Oligocene post-collisional monzonitic intrusions from the Alborz magmatic belt, NW Iran. An example of monzonite magma generation from a metasomatized mantle source. *Lithos.* **180–181**: 109–127 (2013).
- Nabatian G., Ghaderi M., Neubauer F., Honarmand M., Liu X., Dong Y., Jiang S.-Y., von Quadt A., and Bernroder M. Petrogenesis of Tarom high-potassic granitoids in the Alborz-Azerbaijan belt, Iran: Geochemical, U-Pb zircon and Sr-Nd-Pb isotopic constraints. *Lithos.* **184–187**: 324–345 (2014).
- Whitechurch H., Omrani J., Agard P., Humbert F., Montigny R. and Jolivet L. Evidence for Paleocene-Eocene evolution of the foot of the Eurasian margin (Kermanshah ophiolite, SW Iran) from back-arc to arc: Implications for regional geodynamics and obduction. *Lithos.* **182–183**: 11–32 (2013).
- Mohajjal M. and Fergusson C.L. Jurassic to Cenozoic tectonics of the Zagros orogen in northwestern Iran. *Int. Geol. Rev.* **56**: 263–287 (2014).
- Hosseini S.Z. Mineralogy, Geochemistry and Petrogenesis evolution of Pleistocene basaltic lava flows in the Shahre-Babak area, NW of Kerman, Iran: Implication for the evolution of Urumieh-Dokhtar Magmatic Assemblage. Unpublished Ph.D. Thesis, Shahid Bahonar University of Kerman, in Persian. 260 p (2009).
- Hosseini S. Z., Arvin M., Oberhansli R. and Dargahi S. Geochemistry and tectonic setting of Pleistocene basaltic lava flows in the Shahre-Babak area, NW of Kerman, Iran: Implication for the evolution of Urumieh-Dokhtar Magmatic Assemblage. *Journal of Sciences, I.R.of Iran.* **20(4)**: 331–342 (2009).
- Allen M.B. Discussion on the Eocene bimodal Piranshahr massif of the Sanadaj-Sirjan zone, West Iran: A marker of the end of collision in the Zagros orogen. *J. Geol. Soc. London.* **166**: 981–982 (2009).
- Dargahi S., Arvin M., Yuanming P. and Babaei A. Petrogenesis of post-collisional A-type granitoids from the Urumieh-Dokhtar magmatic assemblage, Southwestern Kerman, Iran: Constraints on the Arabian-Eurasian continental collision. *Lithos.* **115**: 190–204 (2010).
- Mouthereau F., Lacombe O. and Vergès J. Building the Zagros collisional orogen: Timing, strain distribution and the dynamics of Arabia/Eurasia plate convergence. *Tectonophysics.* **532–535**: 27–60 (2012).
- Mohajjal M. and Fergusson C.L. and Sahandi, M.r. Cretaceous-Tertiary convergence and continental collision, Sanandaj-Sirjan zone, Western Iran. *J. Asian Earth. sci.* **21**: 397–412 (2003).
- Ali S.A., Buckman, S., Aswad K.J., Jones B.G., Ismail S.A. and Nutman, A.P. The tectonic evolution of a Neo-Tethyan (Eocene-Oligocene) island-arc (Walash and Naopurdan groups) in the Kurdistan region of the northeast Iraqi Zagros suture zone: *Island Arc.* **22**: 104–125 (2013).
- Paul A., Hatzfeld D., Kaviani A., Tatar M. and Péquegnat C. Seismic imaging of the lithospheric structure of the Zagros mountain belt (Iran). *Geol. Soc. Spe. Publ.* **330**: 5–18 (2010).
- Dimitrijevic M.D. Geology of Kerman Region. Geological Survey of Iran, Report Number Yu/52, 334 p (1973).
- Middlemost E.A.K. Naming materials in the magma/igneous rock system. *Earth. Sci. Rev.* **37**: 215–224 (1994).
- Wilson B.M. Igneous Petrogenesis a Global Tectonic Approach. Springer Science & Business Media, 466p. (2007).
- Maniar P.D., and Piccoli P.M. Tectonic discrimination of granitoids. *Geolo. Soc. Ame. Bull.* **101**: 635–643 (1989).
- Zen E.An. Aluminum enrichment in silicated melts by fractional crystallization some mineralogical and petrographic constraints. *J. Petrol.* **27**: 1095–1118 (1986).
- Waught T.E., Weaver S.D. and Muir R.J. The Hohonu batholith of north westland, New Zealand, granitoid compositions controlled by source  $H_2O$  contents and generated during tectonic transition. *Contrib. Mineral. Petr.* **130**: 225–239 (1989).
- Driver L.A. petrogenesis of the Cretaceous Cassiar batholith, Yukon, B.C., Canada: implications for mammatism in the north American Cordilleran Interior. Ms.C. Thesis, Univercity of Alberta, 80 p (1998).
- Rollinson H.R. Using Geochemical Data: Evaluation, Presentation, Interpretation. Pearson Education Limited, London, 317p. (1993).
- Mason b. and Moore C.B. Principles of geochemistry. John Wiley and Sons. 344p (1982).
- Rapp R.P. and Watson E.B. Dehydration melting of metabasalt at 8–32 kbar: implications for continental growth and crust–mantle recycling. *J. Petrol.* **36**: 891–931 (1995).
- Zhong H., Zhu W.G., Hu R.Z., Xie L.W., He D.F., Liu F. and Chu Z.Y. Zircon U-Pb age and Sr-Nd-Hf isotope geochemistry of the Panzhihua A-type syenitic intrusion in the Emeishan large igneous province, southwest China and implications for growth of juvenile crust. *Lithos.* **110**: 109–128 (2009).
- Macpherson C.G., Dreher S.T. and Thirlwall M. F. Adakites without slab melting: high pressure differentiation of island arc magma, Mindanao, the Philippines. *Earth. Planet. Sci. Lett.* **243**: 581–593 (2006).
- Sun S.S. and McDonough W.F. Chemical and isotopic systematics of oceanic basalts: implications for mantle composition and processes. In: Saunders, A.D., Norry, M.J. (Eds.), Magmatism in the Ocean Basins. *Geol. Soc. London Spec. Publ.* **42**: 313–345 (1989).
- Wood D.A., Joron J.L. and Treuil M. A re-appraisal of the use of trace elements to classify and discriminate between magma series erupted in different tectonic settings. *Earth. Planet. Sc. Lett.* **45**: 326–336 (1979).
- Kargadianati T. Petrography, geochemistry and petrogeneses of Baghe Khoske granitoides. North of Sirjan region. Unpublished Ms. C. Thesis, Payame Noor University, in Persian 150 p (2017).
- Haschke, M., Ahmadian, J., Murata, M., McDonald, I., 2010. Copper mineralization prevented by arc-root delamination during Alpine-Himalayan collision in central Iran. *Econ. Geol.* **105**, 855–865.
- Castillo P. R., Janney P. E. and Solidum, R. Petrology and geochemistry of Camiguin Island, southern Philippines: insights into the source of adakite and other lavas in a

- complex arc tectonic setting. *Contrib Mineral. Petr.* **134**: 33–51 (1999).
36. Maury RC, Defant MJ, Joron J-L., 1992. Metasomatism of the sub-arc mantle inferred from trace elements in Philippine xenoliths. *Nature*. **360**: 661–663.
  37. Gill J.B. Orogenic Andesites and Plate Tectonics. Springer-Verlag, Berlin, 390 p (1981).
  38. Dias G. and Leterrier J. The genesis of felsic-mafic plutonic associations: a Sr and Nd isotopic study of Hercynian Braga Granitoid Massif (Northern Portugal). *Lithos*. **32**: 207–223 (1994).
  39. Kuscu, G.G and Geneli, F., 2010. Review of post-collisional volcanism in the Central Anatolian Volcanic Province (Turkey), with special reference to the Tepekoval Volcanic Complex. *Int. J. Earth. Sci. (Geol Rundsch)* **99**: 593–621.
  40. Karsli O., Dokuz A., Uysal I., Aydin F., Kandemir R. and Wijbrans J. Generation of the Early Cenozoic adakitic volcanism by partial melting of mafic lower crust, Eastern Turkey: implications for crustal thickening to delamination. *Lithos*. **114**: 109–120 (2010).
  41. Drummond M.S. and Defant M.J. A model for trondhjemite-tonalite-dacite genesis and crustal growth via slab melting: Archaean to modern comparisons. *J. Geophys. Res.* **95**: 21503–21521 (1990).
  42. Pearce, J.A. Trace element characteristics of lavas from destructive plate boundaries. In: Thorpe RS (ed) Orogenic andesites. Wiley, London, pp. 525–548 (1982).
  43. Dilek Y., Imamverdiyer N. and Altunkaynak S. Geochemistry and tectonic od Cenozoic volcanism in the lesser Caucasus (Azerbaijan) and peri-Arabian collision-induced mantle dynamics and its magmatic fingerprint. *Int. Geol. Rev.* **52**: 536–575 (2010).
  44. Hawkesworth C.J., Turner S.P., McDermott F., Peate D.W. and Van Calsteren, P. U-Th isotopes in arc magmas: implication for element transfer from the subducted crust. *Science*. **276**: 551–555 (1997).
  45. Zhang X., Mao Q., Zhang H., Zhai M., Yang Y. and Hu Z. Mafic and felsic magma interaction during the construction of high-K calc-alkaline plutons within a metacratonic passive margin: the early Permian Guyang batholiths from the northern North China Craton. *Lithos*. **125** (1): 569–591 (2011).
  46. Pearce J.A. Geochemical fingerprinting of oceanic basalts with applications to ophiolite classification and the search for Archean oceanic crust. *Lithos*. **100**: 14–48 (2008).
  47. Rudnick R.L. and Fountain D.M. Nature and composition of the continental crust: a lower crustal perspective. *Rev. Geophy.* **33**: 267–309 (1995).
  48. Rosu E., Seghedi I., Downes H., Alderton D.H.M., Szakacs A., Pecskay Z., Panaiotu C., Panaiotu C.E. and Nedelcu L. Extension related Miocene calc-alkaline magmatism in the Apuseni Mountains, Romania: origin of magmas. *Schweiz. Mineral. Petrogr. Mitt.* **84**: 153–172 (2004).
  49. Shahabpour J. Tectonic evolution of the orogenic belt in the region located between Kerman and Neyriz. *J. Asian Earth. Sci.* **24**: 405–417 (2005).
  50. Pearce J.A., Harris N.B.W. and Tindle A.G. Trace element discrimination diagrams for the tectonic interpretation of granitic rocks. *J. Petrol.* **25**: 956–983 (1984).